Optically controlled electroabsorption modulators for unconstrained wavelength conversion

V. A. Sabnis,[a] H. V. Demir, O. Fidaner, J. S. Harris, Jr., and D. A. B. Miller
Ginzton Laboratory, Stanford University, 450 Via Palou, Stanford, California 94305

J.-F. Zheng
Intel Corporation, M/S SC1-03, 3065 Bowers Avenue, Santa Clara, California 95052

N. Li, T.-C. Wu, H.-T. Chen, and Y.-M. Houng
OEPIC Corporation, 1231 Bordeaux Avenue, Sunnyvale, California 94089

(Received 8 September 2003; accepted 1 December 2003)

We introduce a proof-of-concept, optically controlled, optical switch based on the monolithic integration of a surface-illuminated photodetector and a waveguide electroabsorption modulator. We demonstrate unconstrained wavelength conversion over the entire center telecommunication wavelength band (*C* band) and optical switching up to 2.5 Gbit/s with extinction ratios exceeding 10 dB. Our approach offers both high-speed, low-power, switching operation and two-dimensional array scalability for the fabrication of chip-scale reconfigurable multichannel wavelength converters. © *2004 American Institute of Physics.* [DOI: 10.1063/1.1643539]

All-optical wavelength conversion technologies have recently been extensively investigated to improve the flexibility of wavelength-division-multiplexed optical networks.[1] High-performance optical and optoelectronic techniques that avoid the high packaging costs and performance constraints of traditional optical–electronic–optical conversion have been reported.[2] These techniques, however, offer limited wavelength conversion capabilities or cannot be conveniently scaled for multichannel operation. In this letter, we introduce a dual-diode, optically controlled, electroabsorption modulator that offers bidirectional, unconstrained, wavelength conversion over the entire *C* band (i.e., 1530–1565 nm). The compact size of our device, surface-normal optical control, electrical reconfigurability, and low optical and electrical power requirements allow for single chip implementation of two-dimensional arrays of multichannel wavelength converters.

Figure 1 shows a top view microscope picture of a fabricated switch[3] that includes: (i) a surface-illuminated, InGaAs–InP, *p-i-n* diode photodetector (PD), (ii) a multiple-quantum-well, InGaAsP–InP, *p-i-n* diode waveguide electroabsorption modulator (EAM), and (iii) a TaN thin-film resistor (*R*). The switch is monolithically integrated onto an InP substrate in a 300 μm by 300 μm area. The switch inputs consist of a high-speed optical data stream at λ_1 incident on the PD and a continuous-wave beam at λ_2 incident on the input facet of the EAM. The switch output is the output beam from the EAM. The switch transfers optical data from the incident PD beam to the output beam of the EAM. The PD is capable of broadband photodetection for wavelengths smaller than 1650 nm. The EAM is designed to efficiently modulate wavelengths over the *C* band by appropriately presetting its dc bias point. Hence, the switch is capable of performing unconstrained bidirectional wavelength conversion over the entire *C* band.

A circuit schematic of the device is presented in Fig. 2. The PD and EAM are independently reverse biased and share a common ground connection through the on-chip resistor that connects to the *p* regions of both devices. Bypass capacitors on the bias lines decouple the local high-speed response from the external circuitry and allow the switching bandwidth to be determined by the resistance/capacitance time constant of the PD, EAM, and on-chip resistor. Such a configuration possesses simple electrical packaging requirements since the use of microwave circuitry and expensive rf connectors are eliminated. To operate the switch, a sufficient PD bias is applied to allow for high-speed, linear, photocurrent extraction and a sufficient EAM bias is applied to strongly absorb at the wavelength of the continuous-wave input beam, λ_2. Switching occurs when an optical data stream is incident on the PD, generating a photocurrent, which is then discharged through the on-chip resistor. The photocurrent creates a voltage drop across the resistor, which in turn reduces the applied bias across the modulator. Through the quantum confined Stark effect,[4] this reduction in voltage results in the initially absorbed EAM input to be strongly transmitted through the waveguide. Hence, data are transferred from the PD input beam at λ_1 to the EAM output at λ_2. The switch can be electrically reconfigured by setting

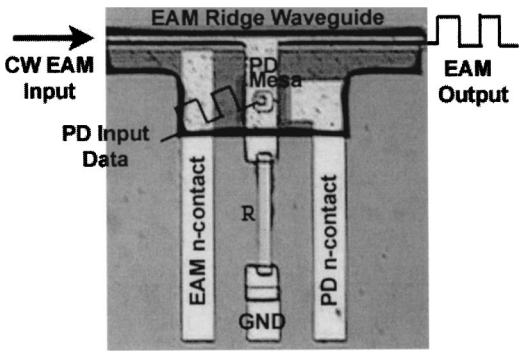

FIG. 1. Top view microscope picture of a fabricated switch.

[a]Electronic mail: vsabnis@snow.stanford.edu

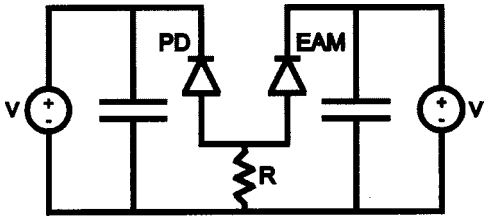

FIG. 2. Simplified circuit diagram of the switch.

the PD bias appropriately. By slightly forward biasing the PD, photocurrent from the incident data stream cannot be extracted, disabling the switching capability. Such a capability, along with the compact size of the switch, enables the realistic fabrication of arrays of these switches for creating a multichannel wavelength-converting crossbar switch.

To compactly integrate the EAM and PD on a single InP substrate, we developed a two-step metalorganic chemical vapor deposition (MOCVD) process using selective area regrowth.[5] The EAM epitaxy was grown on a semi-insulating (Fe-doped) InP substrate and comprised a 1.4 μm thick, *n*-doped, bottom cladding layer, a 0.5 μm thick, undoped, intrinsic region containing ten strained InGaAsP/InGaAsP quantum wells, and a 1.3 μm thick, *p*-doped, upper cladding layer. Ridge mesas were subsequently dry etched into the wafer creating the EAM waveguides that were designed for single transverse mode operation over the *C* band. Silicon nitride (SiN) was then deposited onto the wafer and patterned into 20 μm wide stripes encompassing the waveguides. A second MOCVD growth was used to selectively incorporate the PD epitaxy outside the SiN stripe area. The PD epitaxy comprised a 0.33 μm thick, *n*-doped, InP contact layer, a 1.25 μm thick, InGaAs absorber, a 0.06 μm thick, compositionally graded InGaAsP region used for enhancing hole transport, a 0.15 μm thick, undoped InP layer, and a 0.63 μm thick, *p*-doped InP layer. The selective area growth technique introduced an epitaxial layer thickness enhancement and compositional variation near the SiN mask edge. To avoid these effects, the PD and EAM are fabricated with a 50 μm separation; this small separation allows for high-speed electrical interconnection of the PD and EAM at the operating speeds of interest. Following the PD mesa etch, *n* contacts for both the PD and EAM were evaporated. The PD and EAM were subsequently passivated and planarized using bisbenzocyclobutene. The TaN thin-film resistor was then deposited, followed by evaporation of the *p*-contact metalization. The overall switch was integrated in approximately a 300 μm by 300 μm area, allowing for the possibility of lumped circuit operation up to several tens of GHz. For this proof-of-concept experiment, we fabricated switches with 30 μm$\times$30 μm photodetectors, 300 μm long waveguide electroabsorption modulators with widths ranging from 2–5 μm, and 340 Ω and 650 Ω TaN resistors.

The functionality of the switches was tested first by electrically measuring the current–voltage ($I-V$) curves of an EAM from a particular switch with and without optical excitation of the PD. For example, when the PD generates 5 mA of photocurrent, we found the EAM $I-V$ curve to shift to larger reverse biases by approximately 3.4 V. This optically induced voltage shift agrees well with the expected voltage drop of 5 mA flowing through the 650 Ω on-chip resistor and demonstrates optical control of the EAM voltage. Such a voltage drop across the EAM diode corresponds to a 6.8 V/μm electric-field swing across the multiple-quantum wells, which is more than sufficient to provide for strong optical transmission modulation with extinction ratios exceeding 10 dB.

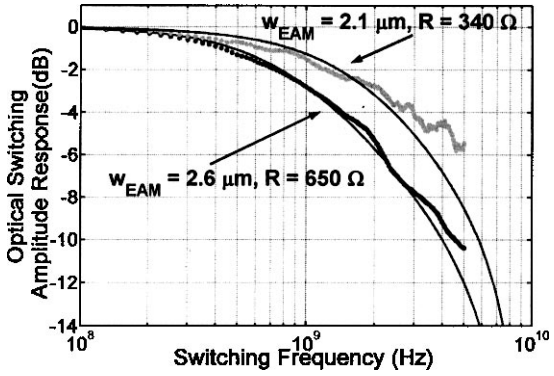

FIG. 3. Experimental and theoretical optical S_{21} transfer functions for two different switch designs.

Figure 3 shows the optical S_{21} amplitude transfer response as a function of optical input modulation frequency for two different device designs, demonstrating 3 dB optical bandwidths of 1 and 2 GHz. Our theoretical model agrees well with the experimental results and confirms the validity of the circuit model presented in Fig. 2. The 1 GHz bandwidth switch corresponded to a 2.6 μm wide EAM waveguide with a 650 Ω resistor, while the 2 GHz bandwidth switch corresponded to a 2.1 μm wide EAM waveguide with a 340 Ω resistor.

For a switch comprising of a 2.65 μm wide EAM and a 650 Ω resistor ($\sim$1 GHz 3 dB bandwidth), Fig. 4 illustrates 1.25 Gbit/s eye diagrams, demonstrating wavelength conversion from 1551.7 nm (PD input) to three exemplary wavelengths (EAM output) across the *C* band. An optically preamplified receiver and digital communications analyzer were used to record the eye diagrams. The coupled EAM input power was approximately 2 mW. The average absorbed PD input power was 5.6 mW, fixed for all cases, and resulted in $>$10 dB rf extinction ratios. There are no constraints on the choice of input wavelengths within standard telecommunication bands because of the wide wavelength photodetection capabilities of the PD. This allows our switch to perform truly arbitrary wavelength conversion over the entire *C* band.

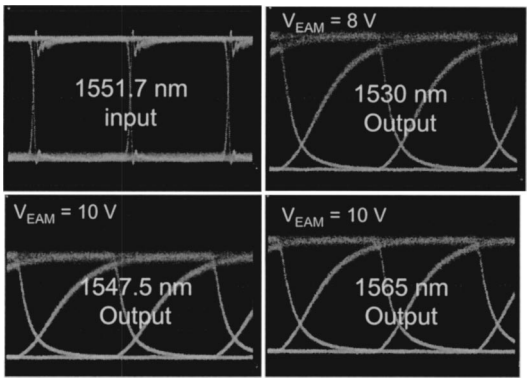

FIG. 4. 1.25 Gbit/s eye diagrams demonstrating full *C*-band wavelength conversion.

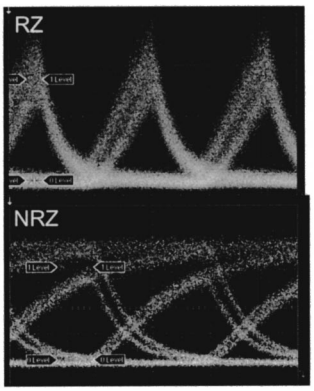

FIG. 5. RZ and NRZ eye diagrams at 2.5 Gbit/s.

Figure 5 shows return-to-zero (RZ) and nonreturn-to-zero (NRZ) 2.5 Gbit/s eye diagrams with >10 dB rf extinction ratios for a switch comprising a 2.1 μm wide EAM and a 340 Ω resistor ($\sim$2 GHz 3 dB bandwidth). The average absorbed PD input power was <8 mW for both the RZ and NRZ cases. In both eye diagrams, a pattern effect is observed, illustrating that the switching bandwidth is nonoptimal for 2.5 Gbit/s operation. Furthermore, the long rise time present in the NRZ case illustrates field-screening effects in the PD, resulting in increased carrier sweepout times. We expect that optimized versions of these devices will result in increased switching bandwidths with smaller required optical switching powers, alleviating the nonidealities present in the eye diagrams shown in Fig. 5. Our theoretical model suggests that switches, operating at 10 Gb/s with greater than 10 dB extinction ratios, are practically feasible, and current work focuses on fabricating such devices.

In conclusion, we have demonstrated a compact, low power, optically controlled, electroabsorption modulator performing unconstrained wavelength conversion up to 2.5 Gbit/s with extinction ratios exceeding 10 dB. Such an architecture is amenable to scalability to two dimensions, allowing the possibility of creating a multichannel wavelength-converting crossbar switch. High-speed operation of these devices at 10 Gbit/s and beyond appears feasible through appropriate optimization of the electroabsorption properties of the EAM multiple-quantum wells and progressive reduction in the size of the on-chip resistor and PD and EAM capacitances.

[1] S. J. B. Yoo, J. Lightwave Technol. **14**, 955 (1996).
[2] K. E. Stubkjaer, IEEE J. Quantum Electron. **6**, 1428 (2000).
[3] H. V. Demir, V. A. Sabnis, O. Fidaner, S. Latif, J. S. Harris, Jr., D. A. B. Miller, J.-F. Zheng, N. Li, T.-C. Wu, and Y.-M. Houng, in *Proceedings of the IEEE Lasers and Electro-Optics Society 2003 Annual Meeting* (IEEE, Piscataway, NJ, 2003), pp. 644–645.
[4] D. A. B. Miller, D. S. Chemla, T. C. Damen, A. C. Gossard, W. Wiegmann, T. H. Wood, and C. A. Burrus, Phys. Rev. Lett. **53**, 2173 (1984).
[5] V. A. Sabnis, H. V. Demir, O. Fidaner, J. S. Harris, Jr., D. A. B. Miller, J.-F. Zheng, N. Li, T.-C. Wu, and Y.-M. Houng, *OSA Integrated Photonics Research* (Optical Society of America, Washington DC, 2003), pp. 12–14.